Article

Not peer-reviewed version

Accompanying Hemoglobin Polymerization in Red Blood Cells in Patients with Sickle Cell Disease Using Fluorescence Lifetime Imaging

Fernanda Aparecida Borges da Silva , Joao Batista Florindo , Amilcar Castro de Mattos , Fernando Ferreira Costa , Irene Lorand-Metze , Konradin Metze *

Posted Date: 3 October 2024

doi: 10.20944/preprints202410.0252.v1

Keywords: fluorescence lifetime imaging; auto-fluorescence; hemoglobin; polymerization; machine learning

 doi:10.20944/preprints202410.0252.v1

Article

Accompanying Hemoglobin Polymerization in Red Blood Cells in Patients with Sickle Cell Disease Using Fluorescence Lifetime Imaging

Running title: FLIM in polymerized hemoglobin

Fernanda Aparecida Borges da Silva [1,2], João Batista Florindo [3], Amilcar Castro de Mattos [1,4], Fernando Ferreira Costa [5], Irene Lorand-Metze [5] and Konradin Metze [1,2,*]

[1] Department of Pathology, Faculty of Medical Sciences, State University of Campinas, SP, Brazil
[2] National Institute of Science and Technology on Photonics Applied to Cell Biology (INFABIC), State University of Campinas, SP, Brazil
[3] Institute of Mathematics, Statistics, and Scientific Computing, State University of Campinas, SP, Brazil
[4] Laboratory of Pathology, Pontifical Catholic University of Campinas PUCC, Campinas, SP, Brazil
[5] Department of Internal Medicine, Faculty of Medical Sciences, State University of Campinas, SP, Brazil
* Correspondence: for correspondence: kmetze@fcm.unicamp.br; +55-19-3521-7379

Abstract: In recent studies it has been shown that fluorescence lifetime imaging (FLIM) may reveal intracellular structural details in unstained cytological preparations which are not revealed by standard staining procedures. The aim of this investigation was to show whether FLIM images could reveal areas suggestive of polymerization in red blood cells (RBCs) of sickle cell disease (SCD) patients. We examined air-dried unstained blood films using auto-fluorescence FLIM images of 45 SCD patients and compared the results with those of 27 control persons without hematological disease. All control RBCs revealed homogeneous cytoplasm without any foci. Rounded non-sickled RBCs in SCD showed between zero and three small intensively fluorescent dots with higher lifetime values. In sickled RBCs we found additionally larger irregularly shaped intensively fluorescent areas with increased FLIM values. These areas were interpreted as equivalent to polymerized hemoglobin. The rounded non-sickled RBCs of SCD patients with homogeneous cytoplasm were not different from those of erythrocytes of control patients in light microscopy. Yet, variables from the local binary pattern transformed matrix of the FLIM values per pixel, showed significant differences between non-sickled RBCs and those of control cells. In a linear discriminant analysis, using local binary pattern transformed texture features (mean and entropy) of the erythrocyte cytoplasm of normal appearing cells, the final model could distinguish between SCD patients and control persons with an accuracy of 84.7% of the patients.When the classification was based on the examination of a single rounded erythrocyte, an accuracy of 68.5% was achieved. Employing the Linear Discriminant Analysis classifier method for machine learning, the accuracy was 68.1%. We believe that our study illustrates the topography of the intracellular polymerization process of hemoglobin in sickle cell disease and that the images are compatible with the theory of the two step nucleation. Furthermore, we think that the presented technique may be an interesting tool for the investigation of therapeutic inhibition of polymerization..

Keywords: fluorescence lifetime imaging; auto-fluorescence; hemoglobin; polymerization; machine learning

1. Introduction

Sickle cell disease (SCD) is a group of inherited diseases defined by mutations in the gene encoding the beta globin chain of hemoglobin, which is the oxygen carrier molecule of red blood cells (RBCs) [1]. This altered hemoglobin has a lower affinity to O_2 and polymerizes in the deoxygenated form, leading to a deformation of RBCs (sickling). These cells have an impaired rheology and a premature hemolysis. The most common disease is sickle cell anemia (homozygous SS), but

 doi:10.20944/preprints202410.0252.v1

hemoglobin S can also be co-inherited with hemoglobin C (hemoglobinopathy SC) or thalassemia (Sβ-thalassemia or Sα-thalassemia). All these disorders have a similar clinical spectrum of vaso-occlusive painful crises and multiple organ damages.

SCD is prevalent in several regions of the world such as Africa, USA and Middle East, and now increasing in Europe. In Brazil, an incidence between 0.15% and 10.9% of the βS allele has been reported[9]. So, an early diagnosis, especially in children and in primary healthcare as well as in blood banking is important.

The key pathophysiological process in SCD is the hemoglobin polymerization, which has been analyzed by a combination of different sophisticated laboratory methods. The majority of the studies have been made in vitro and thus the topographical context of the molecules was lost [1–3]. Furthermore, artefacts may be introduced. In this context, methods based on molecule fluorescence are interesting because they permit to analyze the polymerization process without alteration of the cell topology. Recently, Garcia and Blum have demonstrated that fluorescence lifetime imaging (FLIM) is able to examine the phenomenon of polymerization of molecules in a real time manner [4]. The authors have also shown a direct correlation between polymer fluorescence lifetime and its molecular weight, and could follow morphologically the temporal changes in the polymer architecture over time in a liquid medium. Application of this method for the study of hemoglobin S polymerization could be interesting.

FLIM microscopy permits to create virtual images showing sub-cellular structures not seen in standard preparations [5–11]. The image contrast is built by differences between the fluorescence lifetimes which are captured per pixel of the image. When a molecule is hit by a laser pulse, there is time delay, called fluorescence lifetime before a fluorescence photon will be emitted (fluorescence lifetime). Several molecules are auto-fluorescent, such as FAD, NADH, NADPH, hemoglobin, porphyrins, fatty acids and lipopigments, tryptophan and retinol [5,7,9–11]. This fluorescence is captured by a device which registers the lifetime of individual photons. Mean lifetimes/pixel are calculated and transformed into pseudo-colors, thus creating virtual microscopic images [5]. The lifetime is not only dependent on the chemical composition of the molecule, but also on its environment (pH, pO_2) and conformational changes, including polymerization [5,7,9–11].

As FLIM features may describe the attributes of polymerized proteins, in the present study we tried to investigate whether the phenomenon of hemoglobin polymerization in RBCs of patients with SCD can be examined studying auto-fluorescence and FLIM changes in RBCs in air-dried and unstained peripheral blood smears. In the first step we looked at the simple auto-fluorescence and FLIM images for changes suggestive of polymerization. In a second step we compared fluorescence lifetime data by statistical comparison between cells of SCD patients and control persons without hematological disease and in a third step we searched for texture changes which might not be visible for the human observer at the level of light microscopy, but were able to discriminate between SCD and normal blood cells.

2. Results

Unstained smears of peripheral blood from 45 patients with sickle cell disease (26 cases of SS, 12 cases of SC, 4 patients with S beta-thalassemia and 3 cases of S alfa-talassemia) were compared with those of 27 cases of persons without hematological disease. Median age of the patients was 43 years (17-72); there were 21 men and 24 women. Among the SCD patients 20 were receiving hydroxyurea: 18 of 26 with SS and 2 of 4 with S beta-thalassemia.

We analyzed 10 cells per case in controls and 10 non-sickled cells per patient, but only a mean of 5 sickled cells per smear of patients, since this type was rarely found in some blood films. So, a total of 270 cells from the control group, 450 non-sickled and 214 sickled cells of patients were examined.

The morphological characteristics of the images are shown on Figures 1 (normal RBCs) and patients (Figures 2–4).

 doi:10.20944/preprints202410.0252.v1

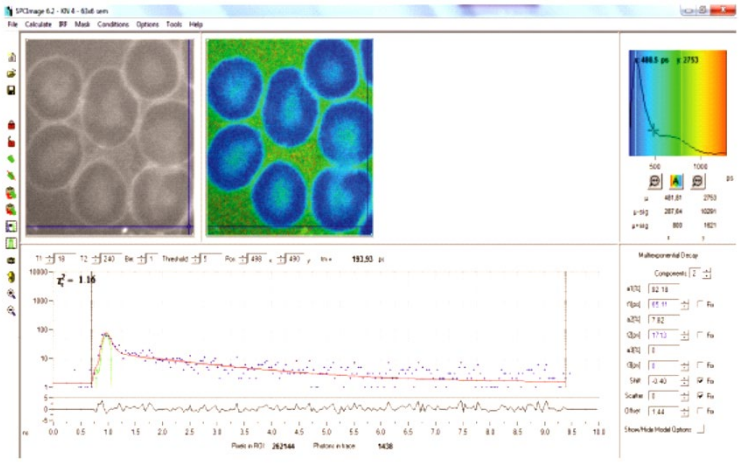

Figure 1. image of a peripheral blood film of a control case with several normal RBCs. Upper left: auto-fluorescence picture. Upper middle: fluorescence lifetime image: the blue color corresponds to the lifetime of hemoglobin. Surrounding plasma in green/yellow color corresponding to a higher lifetime. Upper right: histogram of the lifetime distribution of the image (pseudo-colors according to the rainbow spectrum). Blue represents the shortest lifetime and red is the longest. Below is the fluorescence lifetime decay curve of the selected spot in the image. Every dot represents a single photon.

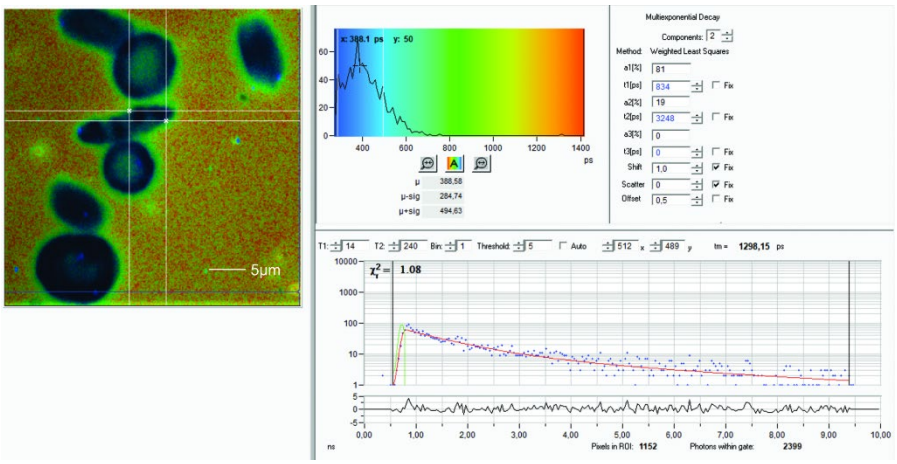

Figure 2. upper left: FLIM image of a patient with homozygous SS hemoglobinopathy. A sickled RBC with parallel areas with a higher fluorescence suggestive of polymerization. The rectangle delineates the maximum possible area of interest where the matrix was extracted for texture analysis. The histogram on the right side represents only the mean lifetime values of each pixel inside the rectangle. Lower right is the decay curve of the selected region of interest.

 doi:10.20944/preprints202410.0252.v1

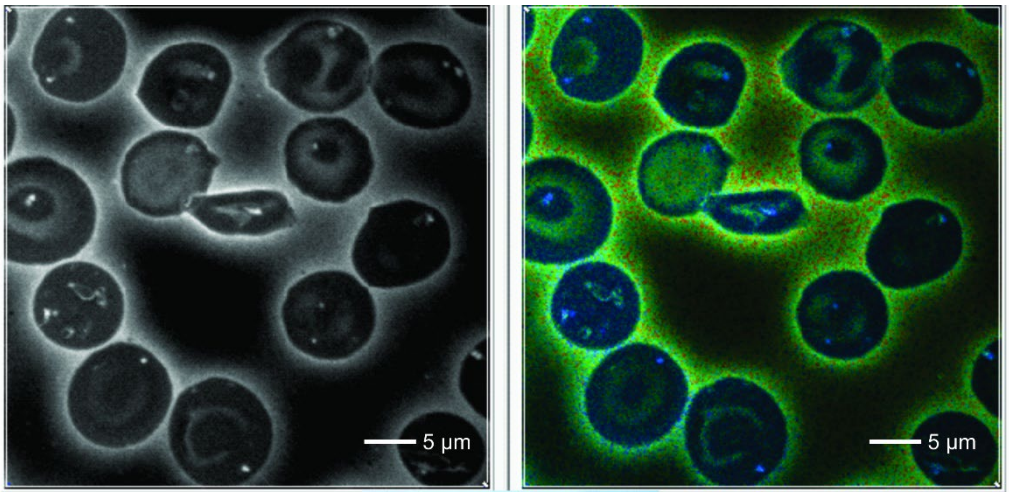

Figure 3. RBCs from a blood smear of a patient with SC hemoglobinopathy. Left: auto-fluorescence and right FLIM image. In the center a sickled cell with an irregular heterogeneous area of enhanced fluorescence revealing a higher lifetime value in the FLIM compared to the surrounding cytoplasm. Some of the non-sickled RBCs show highly fluorescent dots.

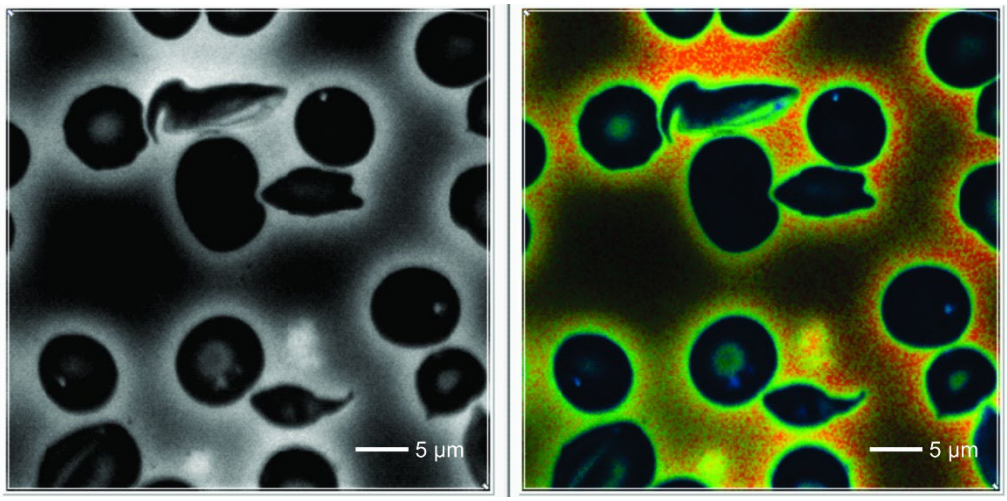

Figure 4. RBCs from a blood smear of S beta-thalassemia hemoglobinopathy. Three entire sickled cells with irregular sometimes heterogeneous areas with enhanced fluorescence revealing higher lifetime values compared to the surrounding cytoplasm. Some of the non-sickled RBCs show highly fluorescent dots.

In control normal RBCs we observed a homogeneous cytoplasm which showed a deep blue color in the default FLIM picture. Interestingly, in SCD one could detect 0-3 small dots (white/bluish in the FLIM images) that were never observed in normal red blood cells. They were also present in sickled cells. These cells also revealed some irregularly shaped large areas adherent to the cell membrane, also intensively fluorescent with increased lifetime values.

Counting the small dots and larger areas together, the total foci per cell increased from normal to sickle shaped RBCs in SCD patients (Figure 4) (mean 0.05 / cell and 1.63 respectively) $p < 0.001$. Considering only sickled cells, the number of dots per cell was highest in patients with Sβ thalassemia $p = 0.04$. There were no significant differences in the number of dots per cell between patients treated with hydroxyurea and those not treated.

Table 1 shows FLIM matrix-derived variables expressed as mean values per patient. The variables “mean”, “standard deviation”, “skewness” and “entropy” of the lifetime histograms were not significantly different comparing SCD patients and controls but reached a high level of

 doi:10.20944/preprints202410.0252.v1

significance when derived from LBP transformation of these variables. No feature was significantly different between SS and SC or S thalassemia and so they were calculated together (Figure 5).

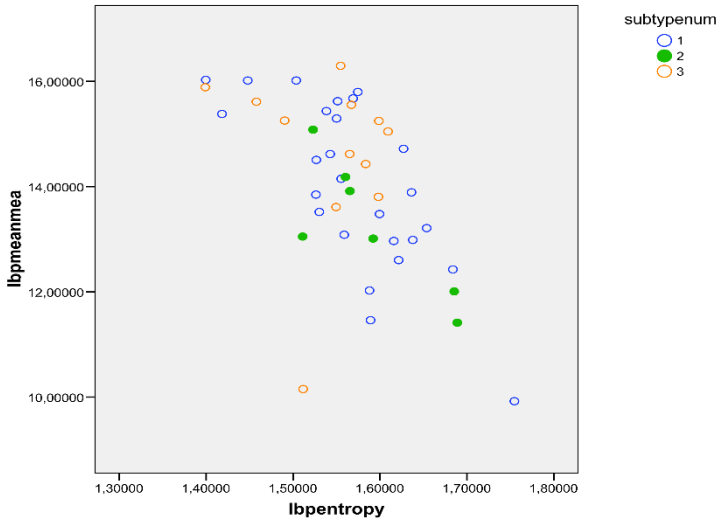

Figure 5. distribution of non-sickled cells in patients with SCD according to the sub-types: SS in black, SC in green and S thalassemia in orange. There were no significant differences among the different sub-types of SCD.

At last, we run a stepwise linear discriminant analysis based on the four variables derived from LBP transformed matrices. The final model contained the variables "LBP mean" and "LBP entropy" with an accuracy of 84.7%. this result dropped to 83.3% after the leave-one-out procedure.

In a further step, we analyzed difference between single cells. Table 2 shows FLIM matrix-derived variables expressed as mean values per cell. Significant differences were found in "mean" and "entropy", and in all variables after the LBP transformation (Figure 6). In the stepwise linear discriminant analysis, a final model was found based on the variables "LBP mean" and "LBP entropy" that yielded an accuracy of 68.5%, which dropped 68.4% after the leave-one-out procedure. Concerning the machine learning algorithm performed according to the Linear Discriminant Analysis classifier (LDA), In this way, we achieved an average F-score of 0.68 ± 0.01. The average accuracy was 68.1%.

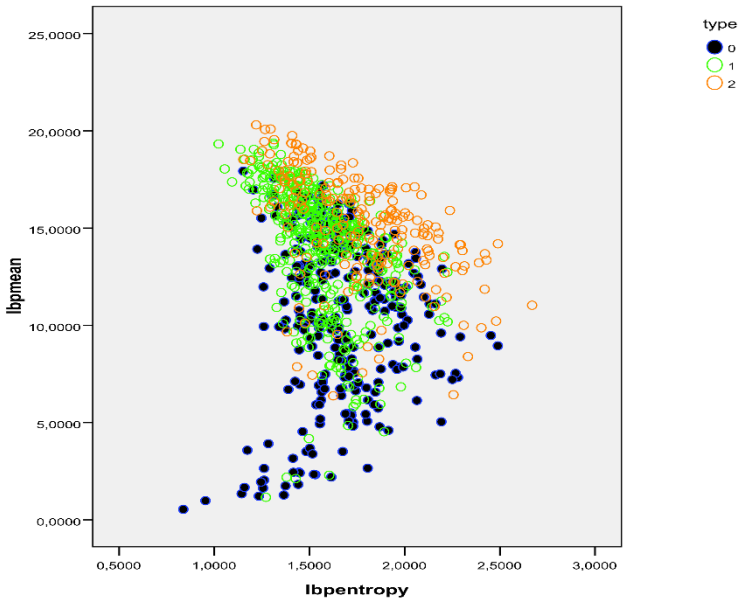

 doi:10.20944/preprints202410.0252.v1

Figure 6. dot plot showing the distribution of LBP mean (Y axis) and LBP entropy (X axis) to show the distribution of each cell in the control group (blue), and SCD: non-sickled cells are in green and sickled cells are in orange. Both parameters were able to discriminate normal and SCD in 84.7% of the cases.

Table 1. mean FLIM values in picoseconds per cases of red blood cells in controls and patients.

	Control cases N=27	P values* Control x not sickled	Non-sickled cells from patients N=45	Sickled cells from patients N=34	P values** Non-sickled x sickled RBCs
mean	175.689	0.31	192.343	247.568	0.000
St. deviation of mean	30.050	0.61	27.702	56.240	0.000
entropy	1.883	0.19	1.8597	1.7884	0.033
skewness	0.801	0.18	0.637	1.033	0.005
LBP					
mean	10.683	0.000	14.063	15.222	0.003
St. deviation of mean	10.284	0.001	10.959	10.498	0.000
entropy	1.675	0.000	1.564	1.721	0.000
skewness	0.649	0.000	-0.1241	-0.300	0.005

Mann-Whitney test: **Wilcoxon test.

Table 2. mean FLIM values in picoseconds per individual red blood cells in controls and patients.

	Controls N=270	P values* Control x not sickled	Patients, not sickled N=432	Patients, sickled N=214	P values* Non-sickled x sickled RBCs
mean	175.531	0.004	193.891	253.335	0.000
St. deviation of mean	30.222	0.49	28.091	58.614	0.000
5%	135.700	0.000	155.050	181.516	0.000
95%	227.679	0.068	243.867	361.172	0.000
entropy	1.886	0.019	1.866	1.807	0.010
skewness	0.787	0.072	0.630	0.950	0.000
LBP					
mean	10.683	0.000	13.981	15.097	0.000
St. deviation of mean	10.284	0.001	10.945	10.475	0.000
entropy	1.675	0.000	1.567	1.766	0.002
skewness	0.649	0.000	-0.103	-0.317	0.000

3. Discussion

Hemoglobin is considered as weakly fluorescent but an auto-fluorescence has been repeatedly shown in cytological or histological preparations [2,8,12–16]. This paradox can be explained by the observation that immediately after an exposure to a light beam, hemoglobin is transformed into a fluorescent photo-product [12]. Cross-linking of fluorescence molecules by aldehydes intensifies the emission of fluorescent photons. Therefore, the post fixation of air-dried blood smears enhances the contrast in the images.

In our material we found dot-like structures with a high FLIM value that were present only in RBCs from patients with SCD. These intensively fluorescent dots were never found in erythrocytes

 doi:10.20944/preprints202410.0252.v1

of controls nor outside of RBCs. We think that they are real structures and not an artefact. The same was true for the irregularly shaped large highly fluorescent areas in sickled cells. The increased lifetimes suggest changes of the molecular structure. It is well known that polymerization of a molecule is associated with an increase of its lifetime values [4]. Therefore, we would like to propose that the intra-cytoplasmatic spots always showing high lifetimes are areas of polymerized hemoglobin.

Hemoglobin polymerization has long been studied in detail. It is a function of HbS concentration, temperature and pH of the solution [1–3,17,18]. The currently favored concept is called the two-step nucleation theory which postulates two rather independent steps: homogeneous nucleation of fibers and their growth. In vitro studies with hemoglobin solutions using interference contrast microscopy have shown the appearance of small globules of about 0.5 micra in diameter as the first microscopically detectable structure. They could correspond to the metastable mesoscopic clusters of deoxygenated hemoglobin S described by Galkin et al. [17]. These small particles can aggregate, elongate and finally form larger structures of polymerized molecules. We think that the intracellular small structures demonstrated in our observation could be equivalent to those small spherulites found in the in vitro studies [3,17]**.** Special attention was drawn to the beginning of the nucleation process. When investigating on the level of the patient comparison, no differences could be found for the lifetime variables mean, standard deviation, skewness or entropy. But after the LBP transformation of the matrices, significant differences between control RBCs and morphologically normal RBCs of SCD patients could be revealed. Finally, the linear discriminant analysis was able to classify correctly about 84% of the cases of patients and controls. These results suggest that subtle changes in the structure of the hemoglobin matrix before major polymerization are not seen by light microscopy and therefore, we believe that our method can accompany the polymerization process and might be useful for laboratory studies.

Our investigation has some limitations. In order to provoke sickling of some cells in the blood samples collected outside a vaso-occlusive crisis, we kept the blood for 24 hours at 4 to 8 degrees Celsius, which is different from the in vivo process. Since the fluorescence of hemoglobin in erythrocytes is based on the formation of a hemoglobin photoproduct during irradiation [12] it would be necessary to investigate the biochemical nature of the fluorescent polymerized hemoglobin in our study. Due to technical reasons it was only possible to extract matrix data inside of a rectangular region of interest which of course is smaller than the whole cytoplasmic area of an RBC, and this represents another limitation. Nevertheless, we could reveal differences of the matrix structures between different cell types. Due to the relatively long exposure time of eight minutes per frame, the number of acquired cells per patient was relatively small. It would be desirable to examine large numbers of non-sickled RBCs in SCD patients in order to see whether there is a transition gradient from the normal cell to the state with dot formation. Furthermore, the limited number of 45 patients is rather small when we are looking for differences in disease subgroups.

Even so, we believe that our study suggests that auto-fluorescence and fluorescence lifetime imaging of unstained blood films of patients with SCD may reveal the topography of the polymerization in RBCs and indicate differences of the molecular structure of the intracellular hemoglobin arrangement before the second phase of the polymerization process. The highly fluorescent dots disclosed in the FLIM image might be a nucleation of the polymerization process.

We believe that our study demonstrates the topography of the intracellular polymerization process of hemoglobin in sickle cell disease and that the images are compatible with the theory of the two-step nucleation. Furthermore, we think that the presented technique may be an interesting tool for the investigation of therapeutic inhibition of polymerization.

4. Material and Methods

4.1. Patients

Our study was approved by the local Ethics Committee (proc. 50809815.7.9995404). Air-dried smears from peripheral blood collected in routine control appointments of SCD patients were examined. After routine peripheral blood counts were made, the sample was stored for 12-24 hours

 doi:10.20944/preprints202410.0252.v1

at a temperature of 4-8 degrees Celsius before a smear was performed. The air-dried slides were fixed by formaldehyde vapor for 1 hour and stored at room temperature [19]. Normal RBCs from patients without a hematological disease were used as control group.

4.2. Techniques

Analysis was made as formerly described [4]. Slides were irradiated by **a** pulsed diode laser (405 nm, 80 MHz). Images were acquired by a confocal Zeiss Upright LSM780-NLO microscope equipped with a 63x oil immersion objective with a ×3 electronic zoom and a HPM-100-40 Hybrid detector (Becker & Hickl). Photons were captured by a photon-counting PMT detector (Becker & Hickl GmbH,Germany) and analyzed by a time-correlated single photon-counting capture card (Becker & Hickl, SPC-830) applying the software SPCM-Single Photon Counter 9.76 and SPCImage 6.2). For each image of 512 x 512 pixels, photons were collected for 8 minutes (according to the recommendation of the manufacturer) in order to get enough photons per pixel and the mean fluorescence lifetime was calculated for each pixel. Then, a virtual FLIM image was constructed by attributing artificial colors to these mean lifetime values (Figure 1), similar to the electromagnetic spectrum of the visible light, starting with blue for the shortest and ending with red for the longest lifetime. At each measurement session, five RBCs from a formaldehyde-fixed reference slide were also measured.

For each RBC examined, we set a rectangle limiting the maximum possible area of interest inside the RBC, strictly avoiding the inclusion of extracellular areas containing plasma. The rectangle defined a matrix containing the mean values per pixels. From these matrices we calculated per cell the mean fluorescence lifetime, its standard deviation, skewness and entropy. In a further step, this matrix was LBP transformed. The new matrix yielded a vector, later used for machine learning. Furthermore we also calculated mean, its standard deviation, skewness and entropy for linear discriminant analysis.

4.3. Local Binary Patterns

Local Binary Pattern (LBP) is a well-established technique to describe digital images, with especial focus on texture images and face recognition [20]. Its straightforward definition and interpretation, as well as the good results achieved in practice, made it a popular tool in classical computer vision (before the popularization of end-to-end deep learning approaches) [21]. Among the reason for that success, one may mention its low computational cost and ability to capture spatial patterns preserving robustness to illumination changes.

The essential idea of LBP is to compare each pixel in the image with its neighbors within a pre-defined radius, assigning *1* if the neighbor pixel has larger intensity than the central pixel and zero otherwise. The LBP code corresponds to that binary representation preserving the order of the neighbor pixels. For practical purposes, that sequence of binary values is converted to decimal representation. Mathematically, in a specific position (x,y) of the image we have

$$LBP_{P,R}(x,y) = \sum_{i=0}^{P-1} s(g_i - g_c)2^i \qquad (1)$$

where R is the neighborhood radius, P is the number of neighboring pixels, g_c is the intensity of the central pixel, g_i is the intensity of the i-th neighboring pixel, and $s(x)$ is an indicator function, such that $s(x)=1$ if $x\geq 0$, otherwise $s(x)=0$. Finally, the image descriptors are provided by the histogram of LBP codes of the image.

Here, in particular, we employ a rotation-invariant uniform version of LBP [22]. To enforce rotation-invariance, the minimum LBP code taken under circular bitwise shifts of the neighborhood is considered. As for the uniformity, a binary pattern is uniform if it contains at most two 0-1 or 1-0 transitions. The uniform version of LBP treats uniform patterns as a unique code in the computation of the histogram. Mathematically, it can be defined by

 doi:10.20944/preprints202410.0252.v1

$$LBP_{P,R}^{riu2} = \begin{cases} \sum_{i=0}^{P-1} s(g_p - g_c)2^i & \text{if } U(LBP_{P,R}) \geq 2 \\ P+1 & \text{otherwise,} \end{cases} \quad (2)$$

where *U* is the uniformity function:

$$U(LBP_{P,R}) = |s(g_{P-1} - g_c) - s(g_0 - g_c)| + \sum_{i=1}^{P-1} |s(g_i - g_c) - s(g_{i-1} - g_c)|. \quad (3)$$

P and *R* are parameters of the method to be defined empirically. Here we adopt *P=24* and *R=3*. The pixel intensities at any real coordinate over the circle with radius *R* are obtained by bilinear interpolation over the pixels effectively present on the original image. Such a procedure gives rise to 26 possible LBP codes, and the descriptors themselves (histogram) correspond to the number of each of these codes in the image. Thus, we have a total of 26 LBP descriptors for each image.

4.4. Linear Discriminant Classifier

We also run the same task with a machine learning algorithm. More specifically we employed the Linear Discriminant Analysis classifier (LDA) [25]. Its primary objective is to find a linear combination of features that best separate the classes. For that, the method assumes that the data from different classes are normally distributed and share the same covariance matrix (but with different means). The goal is to maximize the separation between the means while minimizing the spread within each class. This is done by finding a set of linear boundaries (hyperplanes) that separate the classes. It projects the data into a new lower-dimensional space where the classes are as distinct as possible.

Mathematically, it works by maximizing the Fisher Criterion, defined as:

$$J(w) = \frac{w^T S_B w}{w^T S_W w} \quad (4)$$

where w is the linear transformation vector, SB is the inter-class scatter matrix and SW is the intra-class scatter matrix. LDA chooses a linear combination of features that maximizes this criterion, increasing in this way the class separability. We adopted a hold-out validation scheme (50%/50% for training/testing) and the procedure was repeated 10 times.

4.5. Statistical Analysis

Data were analyzed on two levels. First - cell level: the data represent each cell. Second – patient level: the data represent the mean level of the cells analyzed in that patient. The presence of normal distribution was tested was tested according to Kolmogorov-Smirnov. When comparing sickled and non-sickled cells of SCD patients we used tests for dependent groups and for the comparison to controls tests for independent groups. For group separation we run a stepwise discriminant analysis [23,24] followed by the leave-one-out method in order to avoid overfitting. For statistical analysis Winstat 3.1 and SPSS 22 were used.

Contribution: F.A.B.S collected and analyzed data. ACM has analyzed data and participated in the statistical analysis. JBF has made all the texture analysis and machine learning procedures. I.L.M participated in the study design, reviewed all the images and participated in the statistical analysis and the text elaboration. KM made the study design, was responsible for the technical development, participated in the statistical analysis and reviewed the manuscript.

Acknowledgments: This work was supported by grants from CNPq (573913/2008-0 ; 308975/2014-6 and 131518/2016 -0). JBF and KM participate in the Grant 2020/09838-0 (São Paulo Research Foundation (FAPESP). JBF, FFC and KM have grants from National Council for Scientific and Technological Development, Brazil

 doi:10.20944/preprints202410.0252.v1

(CNPq): JBF: Grants 306030/2019-5 and 306981/2022-0). FFC: Grant 304271/2020-9; K.M.Grant 308192/2022-2. We would like to thank Victor B. Pelegati and Mariana O. Baratti for technical assistance.

Conflicts of interest: The authors state that there are no conflicts of interest to disclose.

References

1. Kato GJ, Piel FB, Reid CD et al. Sickle cell disease. Nature Rev 2022; 4:18010
2. Eaton WA, Bunn HF. Treating sickle cell disease by targeting HbS polymerization. Blood. 2017;129(20):2719-2726
3. Vekilow PG. Sickle-cell haemoglobin polymerization: is it the primary pathogenic event of sickle-cell anaemia? Brit J Haematol 2007; 139:173-184.
4. Garcia IV A., Blum SA. Polymer Molecular Weight Determination via Fluorescence Lifetime. J. Am. Chem. Soc. 2022, 144, 22416−22420
5. Becker, W. Fluorescence lifetime imaging – techniques and applications. *J Microsc* 2012; 247:119-36.
6. Borges da Silva FA, Lorand-Metze, I., Metze, K. Chédiak–Higashi syndrome approached by several different microscopy imaging technologies. *Br J Haematol* 2020, 189 :1001
7. Chacko, JV; Eliceiri, KW. Auto-fluorescence lifetime imaging of cellular metabolism: Sensitivity toward cell density, pH, intracellular, and intercellular heterogeneity. Cytometry Part A 2019;95A:56-69.
8. Borges da Silva FA, Racanelli AP, Lorand-Metze, I., Metze, K. Fluorescence lifetime imaging is able to recognize different hematopoietic precursors in unstained routine bone marrow films. Cytometry Part, A. 2021;99:641–646.
9. Breunig HG, Studier, H., König, K. Multiphoton excitation characteristics of cellular fluorophores of human skin in vivo. *Optics Express* 2010;18:7857-7871
10. Wang HL, Liang XW, Gravot G, Thorling CA, Crawford DHG, Xu ZP, Liu, X., Roberts MS. Visualizing liver anatomy, physiology and pharmacology using multiphoton microscopy. J Biophotonics 2017; 10:46-60.
11. Marcu, L. Fluorescence Lifetime Techniques in Medical Applications. *Ann Biomed Eng* 2012;40: 304–331.
12. Shirshin EA, Evgeny A, Yakimov BP, Boris P, Rodionov SA, Omelyanenko N, Priezzhev, AV, Fadeev VV. Lademann Formation of hemoglobin photoproduct is responsible for two-photon and single photon-excited fluorescence of red blood cells *Laser Physics Letters* 2018;15:075604
13. Metze K, Borges da Silva FA, Racanelli AP. Fluorescence lifetime imaging provides label-free recognition of mucin production in gastrointestinal specimens. *Virchows Arch* 2016; 469:S167-8.
14. Metze, K., Borges da Silva FA. Autofluorescence imaging is useful for the detection of lymph node metastases in unstained paraffin sections. *Virchows Arch* 2017; 471:S249.
15. Metze K, Borges da Silva FA, Racanelli AP, Lorand-Metze, I. Label-free imaging of infectious agents in routine histology and cytology by fluorescence lifetime Imaging (FLIM). *Virchows Arch* 2016; 469:S30.
16. Metze K, Silva FB, Lorand-Metze, I. Label-free light microscopic imaging by auto-fluorescence identifies polymerized hemoglobin in erythrocytes of patients with sickle cell disease. Virchows Arch 2017;(Suplement 1): S138-S138
17. Galkin O, Pan W, Filobelo L, Hirsch RE, Nagel RL, Vekilov PG. Two-step mechanism of homogeneous nucleation of sickle cell hemoglobin polymers. Biophys J 2007: 92:902–913
18. Siow, W., Matthey, F., Bain BJ. The significance of irregularly contracted cells and hemighosts in sickle cell disease. Am J Hematol 2017;92:966–967
19. Jockusch H, Voigt S, Eberhard, D. Localization of GFP in frozen sections from unfixed mouse tissues: Immobilization of a highly soluble marker protein by formaldehyde vapor. J Histochem Cytochem 2003;51:401-404
20. Ojala T, Pietikainen M, Harwood, D. A comparative study of texture measures with classification based on featured distributions. Pattern recognition 1996;29:51–59.
21. Kaur, N., Nazir N., Manik. A review of local binary pattern based texture feature extraction.9th International Conference on Reliability, Infocom Technologies and Optimization (Trends and Future Directions) (ICRITO) IEEE 2021,1–4.
22. Ojala T, Pietikainen M, Maenpaa T. Multiresolution gray-scale and rotation invariant texture classification with local binary patterns. IEEE Transactions on pattern analysis and machine intelligence 2002;24(7):971–987.
23. Cross EM, Chaffin WW: Use of the binomial theorem in interpreting results of multiple tests of significance. Educ Psychol Meas 1982;42:25–34.
24. Lorand-Metze, I; Carvalho, MA; Metze, K. Relationship between morphometric analysis of nucleolar organizer regions and cell proliferation in acute leukemias Cytometry 1998;32:51-56
25. B. Scholkopf and K.-R. Mullert. Fisher discriminant analysis with kernels. In Proceedings of the 1999 IEEE Signal Processing Society Workshop Neural Networks for Signal Processing IX, Madison, WI, USA, pages 41–48, 1999.

 doi:10.20944/preprints202410.0252.v1